JOURNAL OF AIRCRAFT
Vol. 46, No. 2, March–April 2009

Engineering Notes

ENGINEERING NOTES are short manuscripts describing new developments or important results of a preliminary nature. These Notes should not exceed 2500 words (where a figure or table counts as 200 words). Following informal review by the Editors, they may be published within a few months of the date of receipt. Style requirements are the same as for regular contributions (see inside back cover).

Stowability Constraint Within a Two-Dimensional Aerodynamic Optimization Method

M. L. Kolla,* J. W. Yokota,† and J. V. Lassaline‡
Ryerson University, Toronto, Ontario M5M 2K3, Canada
and
I. Fejtek§
Bombardier Aerospace,
Downsview, Ontario M3K 1Y5, Canada

DOI: 10.2514/1.34863

I. Introduction

MULTIDISCIPLINARY constraints were developed for a two-dimensional gradient-based aerodynamic optimization method [1–4]. Thickness constraints [4] and a cross-sectional area constraint [5–7] were added to maintain structural integrity and to optimize for fuel volume, respectively. Curvature constraints [8] were added to control geometric oscillations. This work focuses on implementing a stowability constraint within a high-lift configuration. Significant work has been done on high-lift design optimization. Lin and Dominik [9,10] have focused on designing new high-lift components using both computational methods and wind-tunnel testing. Kim et al. [11] have discussed an adjoint-based method to optimize two-dimensional airfoils using the flap overlap, gap, and shape as design variables. Nemec and Zingg [3] have also discussed results for optimizing high-lift examples using the gap and overlap as design variables. These are necessary, but not the only important, components for the design of an airfoil, especially for high-lift design. As stated by Mathews [12], "The design of high lift systems cannot be based solely upon maximum aerodynamic performance but is constrained by weight, cost, ease of manufacture, maintainability, reliability and the mechanics of the flap movement." Van Dam et al. [13] developed a methodology that merges aerodynamic data with kinematic analysis. This methodology allows a general database of aerodynamic performance to be integrated directly into the mechanism design and analyzed. This Note illustrates how a stowable design space can be created that allows the designer to generate a flap shape that will be stowable. This design space is created by using the path that the flap will take during extension or retraction, which is determined from kinematic analysis. The stowability constraint will provide the designer with another option in high-lift design. This Note only focuses on adjusting the stowable flap shape by having the flap shape as a design variable, but this could easily be incorporated with the flap gap and overlap as design variables.

Received 28 September 2007; revision received 23 September 2008; accepted for publication 3 November 2008.

*Graduate Student, Department of Aerospace Engineering, 350 Victoria Street.
†Associate Professor, Department of Aerospace Engineering, 350 Victoria Street. Member AIAA.
‡Assistant Professor, Department of Aerospace Engineering, 350 Victoria Street. Member AIAA.
§Manager, Core Engineering, 123 Garratt Boulevard. Member AIAA.

II. Linkage System

In traditional kinematic linkage analysis, the parameters are known and the trajectory path is determined. However, in this case, the objective is to determine the linkage parameters so that a desired trajectory path can be achieved. This is known as kinematic synthesis and, due to the number of unknowns, it is an iterative process. Both Norton [14] and Sandor et al. [15] have provided a very detailed kinematic synthesis description for linkages. By using kinematic synthesis, a stowable design space can be created. The first step was to decide on critical but known values that could create the coupler link for the four-bar linkage. Consider Fig. 1: on the main element upper surface, the trailing-edge point is termed the *upper shroud point* $\mathbf{P}_b$. This point is where the flap upper surface and main element meet. Equivalently, there is a lower shroud point $\mathbf{P}_a$ on the main element lower surface that is typically located at about 3% wing chord from the stowed flap leading edge. $\mathbf{P}_1$ is the flap leading-edge location in its extended position. Because the flap chord is fixed throughout the optimization, the flap leading edge in the stowed or cruise position $\mathbf{P}_2$ is known. The rigid-body points are determined using the following equations:

$$P_{1_x} = F_{te_x} - (c_w + \text{tol})\cos\theta_d \qquad P_{1_y} = F_{te_y} + (c_w + \text{tol})\sin\theta_d$$
$$P_{2_x} = (1 - c_w) - \text{tol} \qquad P_{2_y} = 0 \qquad P_{a_x} = P_{2_x} + l_{\text{per}} \tag{1}$$
$$P_{a_y} = M_y(P_{a_x}) + \text{tol} \qquad P_{b_x} = M_{te_x} \qquad P_{b_y} = M_{te_y} - \text{tol}$$

where F_{te_x} and F_{te_y} are the flap trailing-edge coordinates, M_{te_x} and M_{te_y} are the main element trailing-edge coordinates, tol is the manufacturing tolerance and is specified by the designer, l_{per} is the percentage of wing chord at which the lower shroud point will be located and is typically 3%, and c_w is the flap chord length corresponding to the wing chord and is calculated as

$$c_w = c_f \cos\theta_{wf} \tag{2}$$

where c_f is the flap chord and θ_{wf} is the angle between the flap chord and wing chord in the stowed position. The final term θ_d in Eq. (1) is the total flap deflection angle in the extended position, which is

$$\theta_d = \theta_{wf} + \theta_{df} \tag{3}$$

where θ_{df} is the flap deflection angle relative to the flap chord.

The final value represented in Fig. 1, θ_{deg}, is the tangent angle between the main element upper surface and the upper cove line and is specified by the designer. This variable allows for adequate space above the flap for the spoiler to be stored and for manufacturability concerns. During the iterative process, this angle will be checked against the trajectory path, and if this angle is less than the selected value, the process begins again.

Once the coupler points were determined, the flap movement could be modeled as a four-bar linkage. Figure 2 shows the linkage

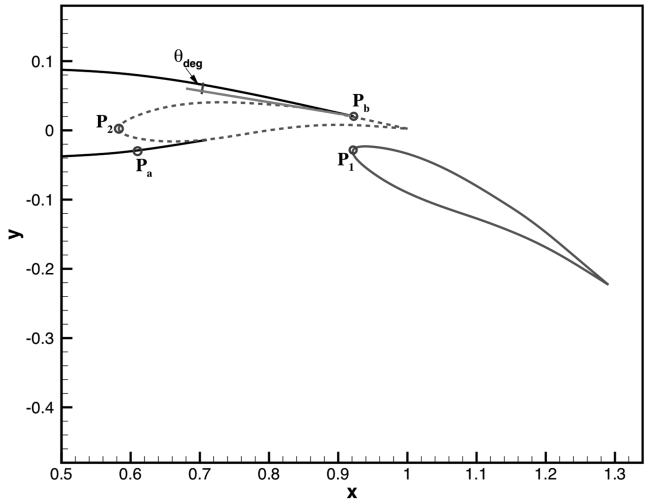

Fig. 1 Essential points for creating the rigid body.

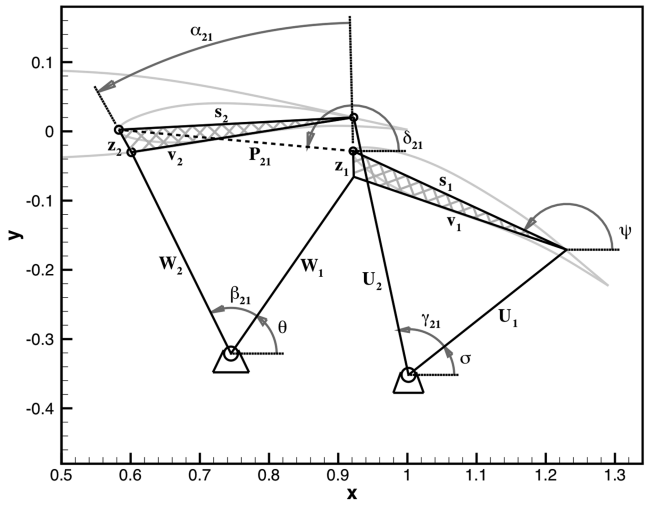

Fig. 2 Four-bar linkage with necessary lengths and angles.

system lengths and angles. The goal is to determine where the pivot points $\mathbf{W}_c$ and $\mathbf{U}_c$ and their corresponding angles θ and σ are located. Begin by solving for the coupler lengths s, z, and v and angles (not shown on diagram) by using the distance equation and the cosine law. Next, the initial and final coupler positions are calculated using the distance equation to solve for P_{21} and angle equations to solve for ψ, ϕ, α_{21}, and δ_{21}. At this point, two angles, β_{21} and γ_{21} are unknown and so the iterative process begins. As an initial first guess, $\beta_{21} = \theta_d$ and $\gamma_{21} = \theta_d + 5$ deg; γ_{21} is initial set 5 deg greater than β_{21} so that the right linkage pivot point will always be ahead of the left point, thereby preventing the linkage arms from colliding.

The pivot points are found by writing a vector loop equation around each pivot point $\mathbf{W}_c$ and $\mathbf{U}_c$, respectively. The vector equation is then rewritten in terms of its complex number equivalents and rearranged into real and imaginary parts to obtain two equations to solve for each pivot point.

With the initial pivot points determined, the trajectory path can be traced from the flap-extended position to its retracted position. However, to create the stowable design area, the path needs to finish past the upper shroud point $\mathbf{P}_b$. Therefore, the trace starts at the angle θ and is incremented through the angle $\beta_{21} + 10$ deg instead of β_{21}. The trajectory path for each coupler point is found using kinematic linkage analysis, as discussed in [14,15]. Once the coupler path has been determined, the last check is performed. The angle θ_{deg} is calculated, and if it is less than the selected value, the iterative process begins again with new values for β_{21} and γ_{21} selected, then new pivot points are calculated, and a new coupler path is finally determined. This process is repeated until θ_{deg} becomes greater than the selected value.

Once the coupler path produces the required θ_{deg}, a design space domain is set up to dictate a stowable flap. On the upper surface between $\mathbf{P_1}$ and $\mathbf{P_d}$, the design space is dictated by the path of $\mathbf{P_d}$ and is hence an arc of radius u_1. The flap lower-surface design space between the lower shroud point $\mathbf{P_c}$ and leading-edge point $\mathbf{P_1}$ is a linear constraint. A linear constraint was used as this exposed area is small and less critical than the upper surface. At the moment, only the surface between the flap lower and upper shroud points is included as a constraint, as it is assumed that the initial flap shape aft of the shroud points meets the main element high-speed lines. Therefore, to complete the design space, a linear constraint was chosen between $\mathbf{P_d}$ and the flap trailing edge and then from the trailing edge to $\mathbf{P_c}$.

The optimization method uses a penalty method to activate the constraint within the objective function. For each point on the flap between P_{1_x} and P_{d_x}, the length r_1 from the pivot point $\mathbf{U}$ to the current point is calculated and compared with the path radius u of $\mathbf{P_d}$. If the length r_1 is greater than the radius u, a penalty is added to the objective function using the penalty method [1]. For the lower surface, each point between P_{1_x} and P_{c_x} is compared with the linear constraint l_1. If the y coordinate of each point is less than l_1, a penalty is added to the objective function.

III. Results

To illustrate this constraint, a single high-lift airfoil configuration and flight condition was chosen. This constraint focuses on modifying the flap surface between the upper and lower shroud points to allow the airfoil to stow within the main element. Because the flap geometries available for two-element configurations already have stowable surfaces, the NLR 7301 [16] two-element configuration was modified and used as the baseline configuration. The two-dimensional gradient-based aerodynamic optimization method development and documented by Nemec and Zingg [1–3] and Nemec [4] was used for testing this example. The freestream conditions are $M_\infty = 0.25, \alpha = 6$ deg, and $Re = 2.51 \times 10^6$, and the flow is assumed to be fully turbulent. The airfoil shape is described with B-spline control points, all of which except the leading-edge point are used as design variables within the design space in this example. The flap was rotated to a landing configuration of 30 deg with a gap of $1.7\%c$ and an overlap of $0\%c$.

As the example presented here is a landing configuration, the optimization goal is to maximize the lift. The convergence criteria is to reduce the norm of the objective function gradient by 3 orders of magnitude. This convergence criteria was selected based on results from previous test cases and from the work done by Nemec and Zingg [3]. The initial lift coefficient is 2.63 and the goal is to increase it by 10% to 2.9. The stowable area for this configuration is based on a flap deflection angle of $\theta_{df} = 30$ deg and a stowed angle between the flap and wing chord of $\theta_{wf} = 4$ deg. A manufacturing tolerance of $\text{tol} = 0.1\%$ was selected.

Two design examples were considered: the first has no constraints and the second has a stowability and thickness constraint. Based on the results from the first design example, the thickness constraint was set to 2.5% chord and located at 40% chord.

The final lift coefficient for both example problems was 2.9 and each converged in 14 and 28 iterations, respectively. The difference between the first and second examples illustrates that the computational cost of the stowability constraint is not significant. The final geometries are shown in Fig. 3.

The first example final geometry exceeds the stowability constraint on the upper surface between 115 and 119% wing chord and just slightly on the lower surface between 94 and 95% wing chord. At the current operating conditions, there exists a high probability that the main element and flap surfaces would collide during flap extension and retraction. By including the stowability constraint in the second example, this concern is removed. To further illustrate the differences between the two examples, consider Fig. 4, which highlights the area around the upper shroud point. It is now clear that the first example exceeds the stowability constraint,

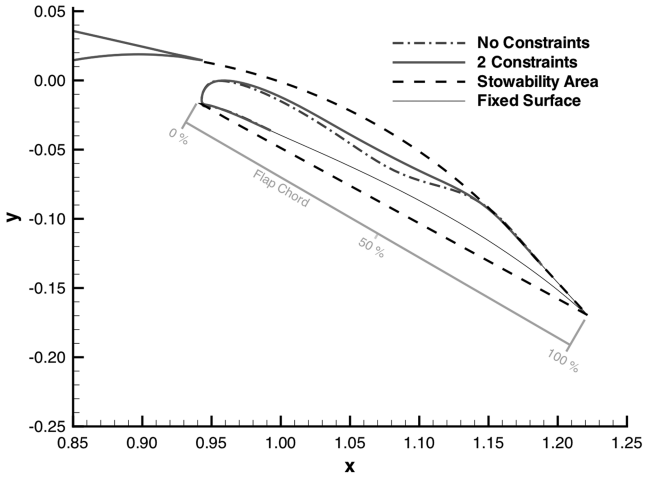

Fig. 3 Final geometries and stowability design area for modified NLR 7301 configuration with no constraints and with a stowability and thickness constraint.

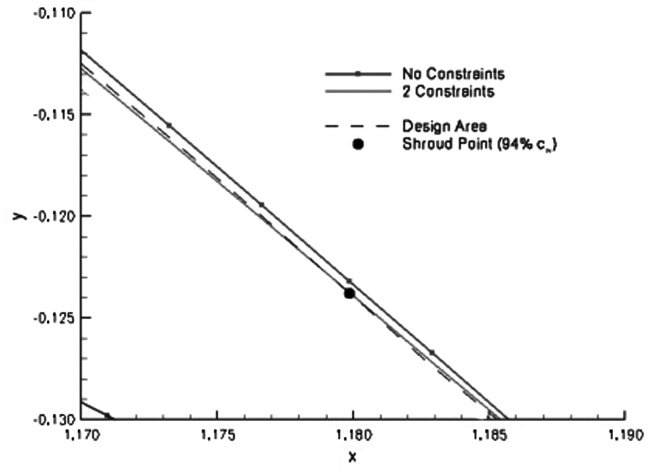

Fig. 4 Geometry and design area near the shroud point for modified NLR 7301 without constraints and a thickness and stowability constraint.

whereas the second example is within the stowability design area. Note that the second example begins to exceed the design area aft of the shroud point; however, this area is not included within the stowability constraint. Visually, the differences may still seem insignificant, but consider this example: the McDonnell Douglas 90 wing [17] has a flap chord of 28 in. and a manufacturing tolerance of 0.01 in. For the example with no constraints, the stowability constraint had a maximum violation of 0.0018% c_f at 91% c_w, and the example with two constraints had a maximum violation of 0.00041% c_f at 96% c_w. If this is applied to the McDonnell Douglas 90 wing, the example with no constraints would exceed the manufacturing tolerance by a factor of 4, whereas the example with two constraints would only exceed the tolerance by a factor of 0.1, which is within the design tolerance.

IV. Conclusions

To summarize, the stowability constraint was demonstrated for a modified NLR 7301 configuration. The stowability constraint influences the flap geometry from the lower-surface shroud point to the upper-surface shroud point. Two design examples were considered, with the second example expanding on the previous results. The first example did not have any constraints placed on the optimization process to determine how the optimization would progress. This example produced a thin flap that exceeded the stowability area. To help resolve these issues, the second example included a thickness and stowability constraint. This example helped to produce a thicker airfoil that could now be safely stowed. By including this stowability constraint, the designer can now include the flap trajectory during the shape optimization process. Future work would include an optimization with the flap shape, gap, and overlap as design variables. Further, a multi-objective example would be of interest, as it would allow for landing, cruise, and takeoff scenarios to be considered.

References

[1] Nemec, M., and Zingg, D. W., "Towards Efficient Aerodynamic Shape Optimization Based on the Navier-Stokes Equations," *15th AIAA Computational Fluid Dynamics Conference*, AIAA Paper 2001-2532, June 2001.

[2] Nemec, M., and Zingg, D. W., "Newton-Krylov Algorithm for Aerodynamic Design Using the Navier-Stokes Equations," *AIAA Journal*, Vol. 40, No. 6, 2002, pp. 1146–1154. doi:10.2514/2.1764

[3] Nemec, M., and Zingg, D. W., "Optimization of High-Lift Configurations Using a Newton-Krylov Algorithm," AIAA Paper 2003-3957, 2003.

[4] Nemec, M., "Optimal Shape Design of Aerodynamic Configurations: A Newton-Krylov Approach," Ph.D. Thesis, Univ. of Toronto, Toronto, 2003.

[5] Venkataraman, P., "Optimal Airfoil Design," 14th AIAA Applied Aerodynamics Conference AIAA Paper 96-2371, June 1996.

[6] Jou, W. H., Human, W. P., Young, D. P., Melvin, R. G., Bieterman, M. B., Hilmes, C. L., and Johnson, F. T., "Practical Considerations in Aerodynamic Design Optimization," 12th AIAA CFD Conference, AIAA Paper 95-1730, June 1995.

[7] Drela, M., *Elements of Airfoil Design Methodology*, Progress in Astronautics and Aeronautics, AIAA, Washington, D.C., 1990, pp. 167–189.

[8] Kolla, M. L., Yokota, J. W., Lassaline, J., and Fejtek, I., "Curvature Constraints for Airfoil Shape Optimization in Turbulent Flow," *Canadian Aeronautics and Space Journal*, Vol. 54, No. 1, 2008, pp. 1–7.

[9] Lin, J. C., and Dominik, C. J., "Optimization of an Advanced Design Three-Element Airfoil at High Reynolds Numbers," *13th AIAA Applied Aerodynamics Conference*, AIAA, Reston, VA, 1995, pp. 779–789; also AIAA Paper 1995-1858.

[10] Lin, J. C., and Dominik, C. J., "Parametric Investigation of a High-Lift Airfoil at High Reynolds Number," *Journal of Aircraft*, Vol. 34, No. 4, 1997, pp. 485–491. doi:10.2514/2.2217

[11] Kim, S., Alonso, J. J., and Jameson, A., "Multi-Element High-Lift Configuration Design Optimization Using Viscous Continuous Adjoint Method," *Journal of Aircraft*, Vol. 41, No. 5, 2004, pp. 1082–1097. doi:10.2514/1.17

[12] Mathews, J. R., "The Aero-Mechanical Design of a Novel Fowler Flap Mechanism," *High-Lift System Aerodynamics*, AGARD CP515, Neuilly-sur-Seine, France, Sept. 1993, pp. 29-1–29-9.

[13] van Dam, C. P., Shaw, S. G., Kam, J. C. V., Rudolph, P. K. C., and Kinney, D., "Aero-Mechanical Design of High-Lift Systems," *Aircraft Engineering and Aerospace Technology*, Vol. 71, No. 5, 1999, pp. 436–443.

[14] Norton, R. L., *Design of Machinery*, McGraw–Hill, New York, 1999.

[15] Sandor, George, N., and Erdman, Arthur, G., *Mechanism Design: Analysis and Synthesis*, Vol. 2, Prentice–Hall, Upper Saddle River, NJ, 1984.

[16] van den Berg, B., and Oskam, B., "Boundary Layer Measurements on a Two-Dimensional Wing with Flap and a Comparison with Calculations," National Aerospace Lab. NLR TR 79009 U, Amsterdam, Jan. 1979.

[17] Rudolph, P. K. C., "High-Lift Systems on Commercial Subsonic Airliners," NASA CR 4746, 1996.